Spectra of energy transport in turbulent channel flows for moderate Reynolds numbers

Yoshinori Mizuno†

Faculty of Science and Engineering, Doshisha University, 610-0394, Kyotanabe, Japan

To reveal the scale dependence of the transport of turbulent kinetic energy in a channel flow, the constituents of a spectral energy budget equation are evaluated using direct numerical simulations. At each height in the buffer and overlap layers, the upward turbulent transport provides energy to the fluctuations at small scales, but removes it from those at large scales. Energy removed from the large scales in the overlap layer is carried upward to the centre of the channel and also downward to the vicinity of the wall. The downward energy fluxes at the large scales result in the well-known anomaly of turbulence intensity and the constituents of the budget equation near the wall. In the overlap layer the cospectrum of the spatial turbulent transport is scaled well by the mixing length. It shows that the structure of fluctuations involved in turbulent transport is self-similar in this layer, supporting the classical assumption. The cospectra of pressure–strain correlations are also evaluated. They are not scaled by the wall unit near the wall, but no symptom of the influence of large-scale structures is observed in the cospectra, at least for the present range of Reynolds numbers. Above the buffer layer the cospectra of the pressure–strain correlations are almost isotropic, and their relevant length scale is given by the mixing length in the overlap layer. The pressure–strain correlations are therefore rather local quantities.

Key words: turbulent boundary layers, turbulent flows, turbulence simulation

1. Introduction

Transport of turbulent kinetic energy is a fundamental process in turbulence. It distributes the energy from the scale and location where it is injected to other scales and locations. This interscale transport results in a broad and continuous energy spectrum. The inhomogeneity of energy injection leads to a net spatial energy transport and determines the spatial profile of turbulence intensity. Wall-bounded turbulent flows are characterised by inhomogeneity in the wall-normal direction, and the turbulent flow region is conventionally divided into two parts. The near-wall region, where the viscosity of the fluid is important, is called the inner layer. The scales obtained using the kinematic viscosity ν and density ρ of the fluid, and friction velocity $u_\tau \equiv \sqrt{\tau_w/\rho}$, where τ_w is the mean shear stress on the wall, are called wall units. They yield relevant scales of flow in the inner layer. In the region away from the wall, called the outer layer, the viscosity has no role, and the relevant length scale

† Email address for correspondence: ymizuno@mail.doshisha.ac.jp

corresponds to that of the flow geometry, for example, the boundary layer thickness or the half-width in channel flows. The turbulent kinetic energy is generated by the interaction of mean shear and tangential Reynolds stresses. It is intense in the inner layer, and some of the injected energy, not dissipated at the location, is delivered toward and away from the wall mainly by turbulent transport. Two important types of turbulent energy transport arise in wall-bounded turbulent flows. One is spatial transport directed away from the wall and the other is interscale transport from large to small scales at each wall distance (Jiménez 1999). An early attempt to resolve the scale dependence of turbulent energy transport is traced back to the work by Lumley (1964), who discussed budget equations for the two-point correlation functions of velocity fluctuations in wall-bounded flows. He assumed that flow structures involved in turbulent transport are self-similar in the logarithmic layer. A model in which spatial and interscale transport and production resulted from the mean shear balance was suggested. Domaradzki *et al.* (1994) evaluated nonlinear transport in the spectral energy budget equation using a few instantaneous velocity fields obtained by direct numerical simulations of wall-bounded turbulent flows. They discussed the energy transfer between wall-parallel scales in Fourier space. Their analysis focused on individual short-time events of energy transfer rather than its statistical nature. A statistical study of energy transfer in a channel flow was carried out by Bolotnov *et al.* (2010). They evaluated the averaged constituents of the spectral energy budget equation using a direct numerical simulation for a marginally low Reynolds number, and revealed the structure of energy transfer in the buffer layer. Orthogonal wavelets were also employed to analyse the spatial and interscale energy transfer in a channel flow (Dunn & Morrison 2003, 2005). They showed that interscale energy transfer occurs both in the forward and backward directions in scale, and is highly intermittent. While in these studies a spectral technique is applied to the two-dimensional fields on the homogeneous wall-parallel plane in order to extract the scale dependence of energy transport on it, the two-point correlations or second-order structure functions of velocity fluctuations may be utilised. Marati, Casciola & Piva (2004) showed that in the logarithmic layer, production and dissipation balance, and upward spatial energy fluxes neither provide nor remove energy at each scale. Following the same direction, Cimarelli, Angelis & Casciola (2013) extracted spiral-like ascending energy fluxes in the composite space of the wall-parallel scales and wall-normal distance, exhibiting inverse (small to large) and then forward (large to small) energy transfer.

An intriguing aspect of wall-bounded turbulent flows is the interaction between the inner and outer layers. The structures of fluctuations in the inner layer may behave autonomously without any interaction with those in the outer layer (Hamilton, Kim & Waleffe 1995; Jiménez & Pinelli 1999), while statistical properties in the outer layer are independent of the details of the inner layer (Flores & Jiménez 2006; Mizuno & Jiménez 2013). On the other hand, it is also well known that the flow in the inner layer is not closed for high Reynolds numbers. For example, the intensities of wall-parallel velocity fluctuations near the wall are not scaled well by the wall unit, and increase with the increase in Reynolds number (DeGraaff & Eaton 2000). This is due to the invasion of large-scale structures of fluctuations in the logarithmic layer into the inner layer (Bradshaw 1967; del Álamo *et al.* 2004). The outer large-scale structures also affect the dynamics of velocity fluctuations in the vicinity of the wall (Mathis, Hutchins & Marusic 2009). These observations imply the existence of downward energy fluxes at large scales, but they have not been discussed until now. The influence of outer large-scale fluctuations on the inner layer has not been clarified in terms of energy transport, though Cimarelli *et al.* (2015) suggested that

the confinement of the inner layer results in the failure of wall scaling of turbulence intensity in the vicinity of the wall. Our present approach is rather classical. We start from a spectral energy budget equation, and represent the contributions as the cospectra of Fourier modes of velocity and pressure fluctuations and Reynolds stresses (Bolotnov *et al.* 2010; Lee 2015; Lee & Moser 2015*b*). One of the objectives of this paper is to reveal the scale dependence of turbulent energy transport.

Pressure–strain correlations in the budget equation for normal Reynolds stresses represent the intercomponent energy transfer. They are actual energy sources for the wall-normal and spanwise components, and their details are important for turbulence modelling. Kim (1989) showed that the pressure–strain near the wall takes its contribution mostly from the near-wall region, whereas that away from the wall takes its contribution from a wide range of the wall distances, that is, globally. These correlations are not scaled by the wall unit near the wall, but are scaled fairly well when the pressure is normalised by the root mean square of the pressure fluctuations (Hoyas & Jiménez 2008). It seems that the failure of the wall scaling of the pressure–strain correlations near the wall is due to that of the pressure fluctuations, but a model for the pressure-related quantities has not been built yet. Spectral information on the pressure–strain correlations will be helpful for the modelling, and will be discussed in the paper as well.

The paper is organised as follows. The spectral energy budget equation is described in § 2. The numerical simulations used to evaluate the constituents of the equation are described in § 3. Turbulent energy transport and pressure–strain correlations are respectively discussed in §§ 4 and 5 and § 6 concludes the paper.

2. Spectral energy budget equation in a channel flow

We consider a pressure-driven incompressible turbulent flow in a channel. The coordinate system used here is the Cartesian system, which consists of the *x*-axis in the streamwise, *y*-axis in the wall-normal and *z*-axis in the spanwise direction. Two solid walls parallel to the *x*–*z* plane are placed at $y = 0$, $2h$. The velocity and pressure are decomposed into their means and fluctuations. The *x*, *y* and *z* components of velocity fluctuation $\boldsymbol{u}$ are denoted by u, v and w, respectively, and pressure fluctuation by p. Owing to the symmetry of the system, the mean velocity has a non-zero component only in the streamwise direction, which depends on *y* and is denoted by $U(y)$ hereafter. For convenience of notation, (u, v, w) and (x, y, z) are sometimes replaced by (u_1, u_2, u_3) and (x_1, x_2, x_3), respectively, in the following.

From the Navier–Stokes equation, one may derive the budget equation for the turbulent kinetic energy $e = (u^2 + v^2 + w^2)/2$ as follows:

$$\frac{\partial \bar{e}}{\partial t} = P + T^p + \Pi + \varepsilon + D, \tag{2.1}$$

where *t* is the time and the overline stands for the averaging over the two homogeneous directions and time. The terms on the right-hand side of the preceding equation are identified as follows:

$$\left. \begin{array}{c} P(y) = -\overline{uv} \dfrac{\mathrm{d}U}{\mathrm{d}y}, \quad T^p(y) = -\dfrac{\mathrm{d}\overline{ev}}{\mathrm{d}y}, \quad \Pi(y) = -\dfrac{1}{\rho} \dfrac{\mathrm{d}\overline{pv}}{\mathrm{d}y}, \\[12pt] \varepsilon(y) = -v \overline{\left(\dfrac{\partial u_j}{\partial x_k} \right)^2}, \quad D(y) = v \dfrac{\mathrm{d}^2 \bar{e}}{\mathrm{d}y^2}, \end{array} \right\} \tag{2.2}$$

where the repeated indices imply summation over 1, 2 and 3. If the flow is statistically steady, the left-hand side of (2.1) vanishes, and the terms on the right-hand side balance each other. The first term $P(y)$ of the right-hand side is the production rate of the turbulent kinetic energy. The energy is first injected to the streamwise velocity component, and then delivered to the other components through the pressure–strain correlations. The second $T^p(y)$ is the spatial turbulent transport. The third term $\Pi(y)$ represents the transport of energy by the turbulent pressure gradient. The fourth and fifth, $\varepsilon(y)$ and $D(y)$, are respectively the dissipation rate and viscous diffusion. Owing to the homogeneity in the wall-parallel directions, the net spatial transport appears only in y, as presented by T^p, Π and D.

   We here consider the spectra of the constituents of (2.1) in each homogeneous wall-parallel plane. The budget equation of the energy spectra is usually obtained by the Fourier transform of the equation of the two-point correlation function of the velocity fluctuation, as in Lumley (1964). However, we may omit this procedure and start from the Navier–Stokes equation of the Fourier modes of the velocity and pressure fluctuations, $(\widehat{u}(\boldsymbol{k}, y), \widehat{v}(\boldsymbol{k}, y), \widehat{w}(\boldsymbol{k}, y))$ and $\widehat{p}(\boldsymbol{k}, y)$, where $\boldsymbol{k} = (k_x, k_z)$ is the wavenumber vector, assuming periodicity in the stream- and spanwise directions. Here $\widehat{}$ stands for the Fourier coefficients that have been transformed only in the x and z directions. To eliminate the effect of the finiteness of the numerical domain on the internal flow dynamics the periods in the homogeneous directions must be large enough. The budget equation of the energy spectrum $\widetilde{e} = \langle |\widehat{u}|^2 + |\widehat{v}|^2 + |\widehat{w}|^2 \rangle / 2$ may then be derived as follows:

$$\frac{\partial \widetilde{e}}{\partial t} = \widetilde{P} + \widetilde{T}^p + \widetilde{\Pi} + \widetilde{\varepsilon} + \widetilde{D} + \widetilde{T}^s, \tag{2.3}$$

where

$$\widetilde{P}(\boldsymbol{k}, y) = \mathrm{Re}\left\{ -\langle \widehat{u}\widehat{v}^* \rangle \frac{\mathrm{d}U}{\mathrm{d}y} \right\}, \tag{2.4}$$

$$\widetilde{T}^p(\boldsymbol{k}, y) = \mathrm{Re}\left\{ -\frac{1}{2} \frac{\mathrm{d}\langle \widehat{u_j}(\widehat{u_j v})^* \rangle}{\mathrm{d}y} \right\}, \tag{2.5}$$

$$\widetilde{\Pi}(\boldsymbol{k}, y) = \mathrm{Re}\left\{ -\frac{1}{\rho} \frac{\mathrm{d}\langle \widehat{v}\widehat{p}^* \rangle}{\mathrm{d}y} \right\}, \tag{2.6}$$

$$\widetilde{\varepsilon}(\boldsymbol{k}, y) = -2\nu(k_x^2 + k_z^2)\widetilde{e} - \nu \left\langle \left| \frac{\partial \widehat{u_j}}{\partial y} \right|^2 \right\rangle, \tag{2.7}$$

$$\widetilde{D}(\boldsymbol{k}, y) = \nu \frac{\mathrm{d}^2\widetilde{e}}{\mathrm{d}y^2}, \tag{2.8}$$

$$\widetilde{T}^s(\boldsymbol{k}, y) = \mathrm{Re}\left\{ \langle \partial_k \widehat{u_j}(\widehat{u_j u_k})^* \rangle - \frac{1}{2} \frac{\mathrm{d}\langle \widehat{u_j}(\widehat{u_j v})^* \rangle}{\mathrm{d}y} \right\}, \tag{2.9}$$

and $(\partial_1, \partial_2, \partial_3) = (ik_x, \partial/\partial y, ik_z)$. The superscript $*$ denotes the complex conjugate, and the brackets $\langle\ \rangle$ denote averaging in time. The constituents (2.4)–(2.8) of the spectral budget equation (2.3) correspond to the decompositions into the spectra or cospectra of the terms on the right-hand side of (2.1), respectively. The last term $\widetilde{T}^s$ defined

by (2.9) represents turbulent energy transport between scales, which does not make any contribution to the total budget (2.1); that is,

$$\sum_{k} \widetilde{T}^{s}(\boldsymbol{k}, y) = 0, \tag{2.10}$$

for any y. It should be noted that there are multiple ways to split the nonlinear transport terms into spatial and interscale parts, such as (2.5) and (2.9). For example, T^{p} may also be decomposed differently from (2.5) as

$$\sum_{k} \mathrm{Re} \left\{ -\frac{1}{2} \frac{\mathrm{d} \left\langle \widehat{(u_{j} u_{j})} \widehat{v}^{*} \right\rangle}{\mathrm{d}y} \right\}, \tag{2.11}$$

leading to an expression different from (2.9) for the interscale transport.

   All the spectra and cospectra in (2.4)–(2.9) retain an explicit y-dependence, and yield no information on the scales in the wall-normal direction. In general, the energy distribution on the scales in the wall-normal direction and the energy transfer between these scales are also important for understanding the physics of wall-bounded turbulent flows, but they will not be discussed here as they are outside the scope of the present work. An attempt to resolve the energy distribution on the wall-normal scales is found in Cimarelli *et al.* (2016).

3. Direct numerical simulation (DNS) and validation

   The constituents of the budget (2.1) as functions of the wall distance in a channel flow have been evaluated by numerical data since the pioneering work of DNS (Kim, Moin & Moser 1987; Mansour, Kim & Moin 1988), and are now accessible for a wide range of Reynolds numbers (Hoyas & Jiménez 2008; Lee & Moser 2015a), but not for their spectral version (2.3). To evaluate (2.4)–(2.9), DNSs of fully developed turbulent channel flows for several Reynolds numbers were carried out. The size of the numerical domain is $L_x \times L_y \times L_z = 32\pi h \times 2h \times 2\pi h$ in common to all the simulations. For spatial discretisation, the Fourier spectral method is employed for the wall-parallel directions and an eighth-order compact finite difference scheme on a non-uniform grid for the wall-normal direction. A semi-implicit three-step third-order Runge–Kutta scheme was used for time marching. Other parameters of the simulations are summarised in table 1. For Re_τ approximately above 500, a self-similar overlap layer can be identified even if an actual logarithmic layer is not observed. The relevant length scale in this layer is given by the mixing length $\ell_m \equiv (\mathrm{d}U^+/\mathrm{d}y)^{-1}$ that tends to κy, where κ is the Kármán constant, for sufficiently high Reynolds numbers (Mizuno & Jiménez 2011). We will also discuss the scaling of the constituents in the overlap layer as a putative logarithmic layer for high Reynolds numbers. The spanwise dimension must be larger than $3h$ to prevent the spatial periodicity from affecting the internal flow dynamics (Flores & Jiménez 2010). Long structures of streamwise velocity fluctuations are typically observed in the logarithmic layer for high Reynolds numbers in wall-bounded flows. The typical length of these structures are known to be $O(10h)$ (del Álamo *et al.* 2004; Hutchins & Marusic 2007; Monty *et al.* 2007), but the longest ones could be $\approx 100h$ (Lozano-Durán & Jiménez 2014a). The computational domain of the present channels is so long that it can capture such very long structures. The present channel is large enough to eliminate the artefact arising from the finiteness of the numerical domain.
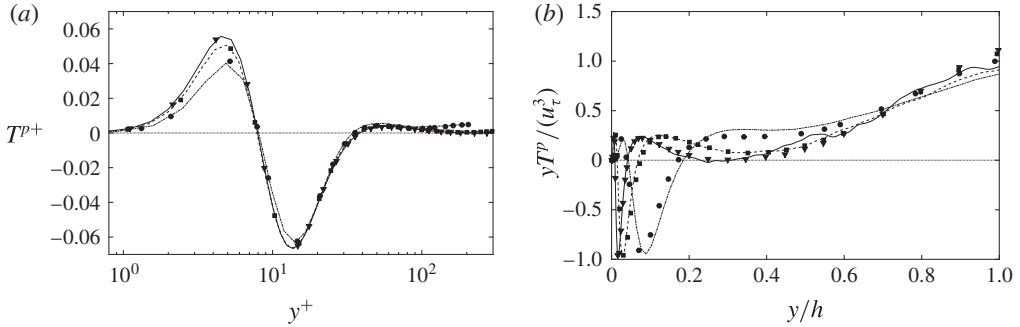
FIGURE 1. Turbulent energy transport in the wall-normal direction $T^p(y)$ in (*a*) inner and (*b*) outer scales. The symbols are the present channels as in table 1. The lines are DNS for $Re_\tau = 180$ (— · —), 550 (——) and 950 (——) by del Álamo *et al.* (2004).

	$N_x \times N_y \times N_z$	Δ_x^+, $\max_y(\Delta_y/\eta)$	Re_τ	Tu_τ/h	Symbol
C200	$4096 \times 129 \times 256$	5.07, 1.23	207	210	●
C500	$8192 \times 257 \times 512$	6.08, 1.17	496	34	■
C900	$16\,384 \times 513 \times 1024$	5.60, 0.914	912	7.3	▲

TABLE 1. Parameters of the present simulations. N_x and N_z are respectively the numbers of the collocating points in the streamwise and spanwise directions, and N_y is the number of grid points in the wall-normal direction. η is Kolmogorov's length scale and $Re_\tau \equiv u_\tau h/\nu = h^+$ is the friction Reynolds number, where the superscript stands for the normalisation by a wall unit. The statistics are compiled during the time T. Δ_x is the spatial resolution in terms of Fourier modes and Δ_y is the grid spacing of the compact finite difference. The spanwise resolution is the same as the streamwise one.

Figure 1(*a*) shows the profiles of spatial turbulent transport $T^p(y)$ in the wall unit, focussing on its behaviour in the inner layer. The profiles for the two higher Reynolds numbers agree quite well up to $y^+ \approx 200$, except for $y^+ = O(1)$, where T^p increases with the Reynolds number. As is already known, the spatial energy fluxes are bifurcated into upward and downward directions at the location $y^+ \approx 15$, where production is most intense. In the figure, the present cases are also compared with a database from another series of DNS of channel flows (del Álamo *et al.* 2004), and are found to agree with them. The long numerical domain in the present cases makes no difference in these one-point statistics in the inner layer, as discussed by Lozano-Durán & Jiménez (2014*a*). Figure 1(*b*) highlights the outer scaling of $T^p(y)$. In this figure T^p is multiplied by y to emphasise its profile in the outer layer. This shows that C500 and C900 agree well above $y/h \approx 0.5$. In particular, the present cases show that the profile is scaled well in the outer layer with u_τ and h. As well as turbulence intensity, the inner and outer scaling works well for the spatial turbulent transport $T^p(y)$, except for the vicinity of the wall.

4. Turbulent energy transport

By turbulent transport, the energy is distributed to different scales and locations from where it is injected. In this section, turbulent energy transport is discussed with an emphasis on its scale dependence.
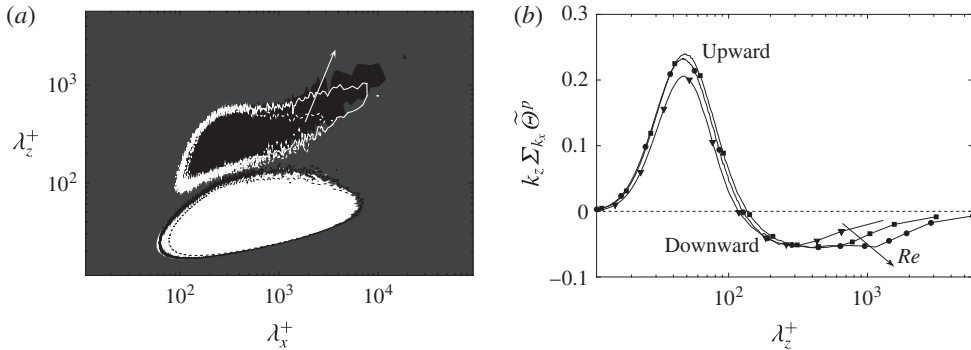
FIGURE 2. (*a*) Premultiplied two-dimensional cospectra of the energy flux in the wall-normal direction, $\widetilde{\Theta}^p$, at $y^+ = 15$. Shaded, C900; ——, C500; — —, C200. Bright (dark) colour indicates positive (negative) levels. (*b*) Premultiplied one-dimensional cospectra of the flux as functions of λ_z. The symbols indicate the Reynolds number as shown in table 1.

4.1. *Inner layer*

In the viscous sublayer where $y^+ = O(1)$, the main contribution to the energy budget is the viscous effects. Because the energy production from the mean shear is weak, the viscous and turbulent transport from the upper locations are the source of energy in this region. The provided energy is dissipated at the same scales as those of the transport (Marati *et al.* 2004). It is known that the total dissipation rate in this region in the wall unit increases with the Reynolds number. This effect of Reynolds number is due to the penetration of large-scale structures in the logarithmic layer into the vicinity of the wall (Hoyas & Jiménez 2008). This will be discussed later in the context of turbulent energy transport.

At $y^+ \approx 15$, the energy production from the mean shear is most intense. Some of the generated energy is carried to slightly smaller scales and dissipated at this location. The remaining energy is carried to upper and lower locations mainly by turbulent transport, as seen in figure 1(*a*). Figure 2(*a*) shows the two-dimensional cospectra of the wall-normal turbulent fluxes

$$\widetilde{\Theta}^p(\boldsymbol{k}, y) = - \int_0^y \widetilde{T}^p(\boldsymbol{k}, y') \, \mathrm{d}y' \qquad (4.1)$$

at $y^+ = 15$ as functions of the wavelengths $\lambda_x = 2\pi/k_x$ and $\lambda_z = 2\pi/k_z$ for the three present cases. The cospectrum of downward fluxes for higher Reynolds numbers has a longer tail extending toward larger scales up to $\lambda_x = O(10h)$ and $\lambda_z \approx h$. Figure 2(*b*) compares the one-dimensional cospectra of the fluxes, $\sum_{k_x} \widetilde{\Theta}^p$, at $y^+ = 15$ for the same cases. It shows that the cospectrum up to $\lambda_z^+ \approx 300$ is universal. The flow structures driving these energy fluxes are commonly observed for all the Reynolds numbers. In contrast, the tail on the larger side grows wider with increasing Reynolds number.

The upward and downward energy fluxes whose scales are independent of Reynolds number compensate for the energy excess at $y^+ \approx 15$ and $\lambda_z^+ \approx 100$, while the downward energy fluxes at large scales carry energy from further upper locations toward the vicinity of the wall. All the downward fluxes end in the viscous sublayer, approximately around $y^+ \approx 5$ (see figure 3*a*). As the Reynolds number increases, the
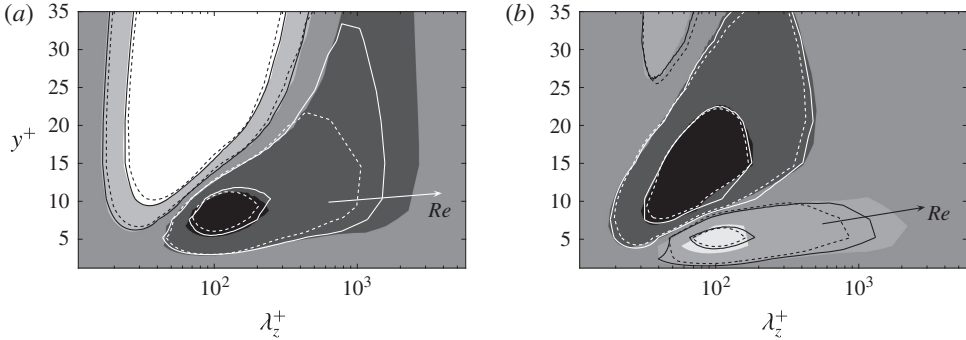
FIGURE 3. Contours of the premultiplied one-dimensional cospectra of (*a*) $k_z \sum_{k_x} \widetilde{\Theta}^p$ and (*b*) contribution of $k_z \sum_{k_x} \widetilde{T}^p$, as functions of the spanwise wavelength λ_z and the wall distance *y*. Shaded, C900; ——, C500; — —, C200. Bright (dark) colour indicates positive (negative) levels. On the contrary, black (white) lines indicate positive (negative) levels.
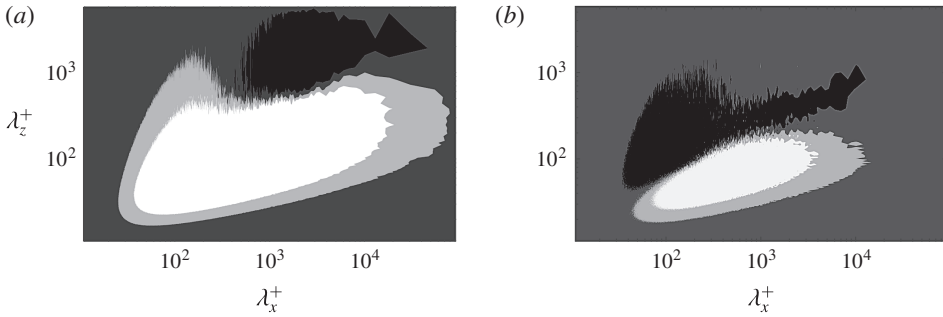

FIGURE 4. Premultiplied two-dimensional cospectra of (*a*) $\widetilde{\Theta}^p$ and (*b*) $\widetilde{T}^p$ at $y^+ = 54$ for C900. White (black) indicates positive (negative) magnitude.

fluxes supply more energy at larger scales, as shown in figure 3(*b*). As will be shown later, this accumulation of energy at large scales causes the failure of the wall scaling of $T^p(y)$ near the wall seen in figure 1(*a*), the enhancement of dissipation rate beside the wall (Bradshaw 1967; Hoyas & Jiménez 2008) and turbulence intensity (DeGraaff & Eaton 2000; Metzger & Klewicki 2001; del Álamo *et al.* 2004) with increasing Reynolds number. As expected, the outer large-scale motions affect the dynamics of velocity fluctuations at this location as well (Mathis *et al.* 2009).

Above $y^+ \approx 20$ in the inner layer, the main contributors to the budget are production, turbulent transport and dissipation, although spatial turbulent transport is relatively weaker than the other contributors. The relevant length scales of production start separating from those of dissipation, and interscale transport carries energy from the former to the latter. Figure 4(*a*) shows the premultiplied two-dimensional cospectrum of $\widetilde{\Theta}^p$ at $y^+ = 54$, as a representative in the buffer layer. As indicated by this figure, the energy fluxes are directed upward at almost all the scales, except at very long and wide scales. As seen from figure 4(*b*), which places the cospectrum of $\widetilde{T}^p$ at the same location as 4(*a*), fluctuations at narrower scales receive energy from the lower fluctuations at the same scales through these upward fluxes, while fluctuations at wider scales lose energy, giving to the upper ones.
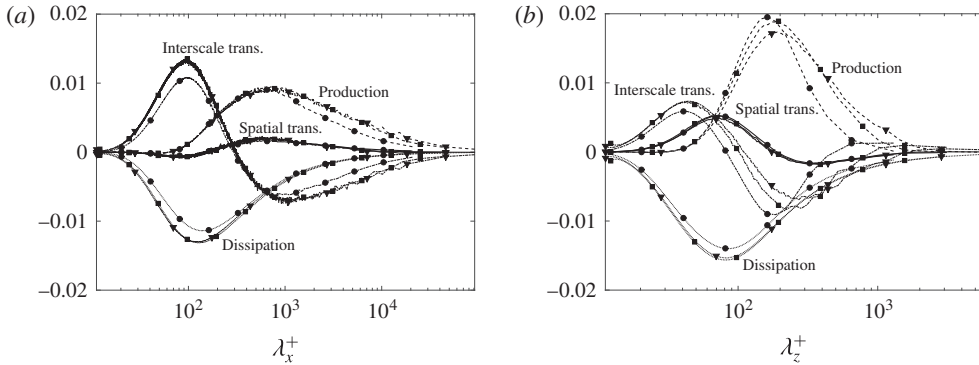
FIGURE 5. Premultiplied one-dimensional cospectra at $y^+ = 60$ as functions of (*a*) λ_x and (*b*) λ_z. ——, production rate; $\cdots\cdots$, dissipation rate; — $\cdot$ —, spatial transport; ——, interscale transport. The symbols indicate the Reynolds number as shown in table 1.

The downward fluxes at large scales are located upstream of those observed at $y^+ = 15$ in figure 2(*a*). These downward fluxes do not provide or drain energy in the buffer layer, but they just carry energy toward the vicinity of the wall. As expected from figure 2, the total intensity of these downward fluxes is weaker for lower Reynolds numbers.

Figure 5 gives the premultiplied one-dimensional cospectra of the main contributors to the budget equation in the buffer layer. If they are plotted as functions of λ_x, as in figure 5(*a*), the contribution from the spatial transport is quite weak compared to the other contributions. The reason for this is clear from the two-dimensional cospectrum shown in figure 4(*b*), which shows that the positive and negative contributions cancel out when summed along the spanwise wavenumber k_z for each λ_x. It is also observed that the profiles for the two higher Reynolds numbers C500 and C900 agree for each constituent. This implies that these cospectra in the wall unit are independent of the Reynolds number in the buffer layer. When plotted as functions of λ_z, the role of spatial turbulent transport is visible, as seen in figure 5(*b*). The cospectrum of the spatial turbulent transport is scaled well by the wall unit. That is consistent to that only the upward fluxes contribute to the budget. The large-scale downward fluxes do not contribute to the budget, but activate production at large scales. Therefore, the cospectrum of the production rate broadens toward larger wavelengths as the Reynolds number increases, and the interscale turbulent transport has wider spectra as well to compensate the energy production at large scales. The streamwise length of the large-scale motions probably does not depend on the Reynolds number, which leads to the weak *Re* dependence of the one-dimensional cospectrum of the production rate as a function of λ_x in figure 5(*a*). At each level, the upward fluxes provide energy at $\lambda_z^+ \approx 100$, which is the typical spanwise length scale of flow structures in the buffer layer.

4.2. *Outer and overlap layers*

Around the centre of the channel, the mean shear and energy production become weak, and spatial turbulent transport supplies energy instead. Above $y/h \simeq 0.7$ the total production and spatial transport are comparable, and at the centre of the channel the gain from spatial transport and dissipation balance, being connected in scales by the interscale turbulent transport.
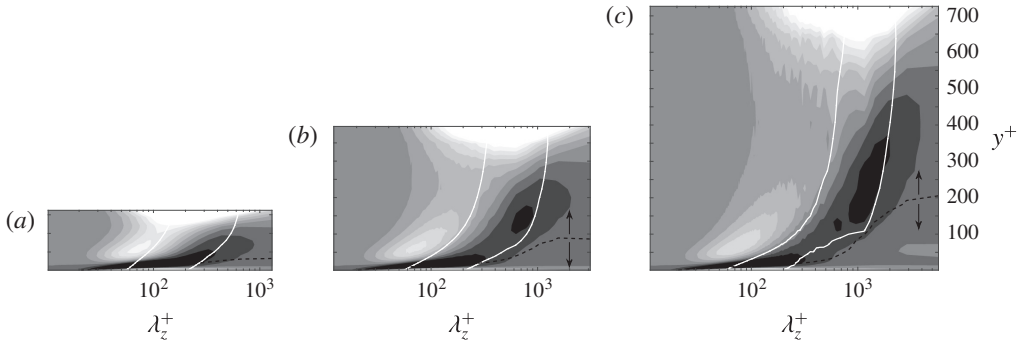
FIGURE 6. Premultiplied one-dimensional cospectra $k_z \sum_{k_x} \widetilde{T}^p$ as functions of λ_z^+ and y^+ for (*a*) C200, (*b*) C500 and (*c*) C900. They are normalised by the total production at each height. Dashed lines are the contours of $\sum_{k_x} \widetilde{\Theta}^p = 0$, and the arrows indicate the direction of the flux. White (black) indicates positive (negative) magnitude. Two white lines in each figure are contours of the energy spectrum, enclosing energy-containing scales.

With the increase in the Reynolds number, the inner and outer length scales separate more from each other. A region where the inner and outer layers overlap then arises, and the so-called logarithmic layer appears in the core of that region for high Reynolds numbers. The present Reynolds numbers are not sufficiently high, but a self-similar intermediate layer still exists for, at least, the higher two cases (Mizuno & Jiménez 2011). Figure 6 shows the rise of the overlap layer where the similarity of spatial turbulent transport is expected. The spatial energy fluxes emanate from the 'watershed' on which the fluxes are zero, shown by dashed lines in the figure. The highest location of the watershed is $y \approx 0.2h$ at $\lambda_z^+ = O(10^3)$ independent of the Reynolds number, and above that all the fluxes are directed upward, carrying energy toward the centre of the channel. The large-scale downward fluxes observed in the inner layer originate in this watershed in the overlap layer.

4.2.1. *Scaling*

The overall picture of the energy budget in the overlap layer is qualitatively similar to that in the buffer layer, but the relevant length scales of the constituents vary with the wall distance *y*. As already known for high Reynolds numbers, the scale of the structures of *uv* is proportional to *y* in the logarithmic layer (Lozano-Durán, Flores & Jiménez 2011), while that of dissipation is proportional to the Kolmogorov's length scale $\sim y^{1/4}$ (Tennekes & Lumley 1972). These scales therefore separate more as they move further away from the wall, and the interscale turbulent transport bridges these separating scales (Jiménez 2012).

Figure 7(*a*) shows the one-dimensional cospectra of the production rate, and spatial and interscale turbulent transport for C900 in the range of $y^+ > 100$ and $y/h < 0.3$, which an overlap layer is assumed to span. As indicated by the arrows in this figure, the relevant length scales of all these contributions increase with the wall distance, while the larger side $y \approx h$ collapses in the outer length scale *h*. In the overlap layer, the length scale of the energy-containing eddies is given by ℓ_m (Mizuno & Jiménez 2011). As shown in figure 7(*b*), the scales, at which those contributions are intense, indeed collapse well if the wavelength is normalised by ℓ_m. Only the smaller side of the interscale turbulent transport shifts toward the smaller wavelength because it
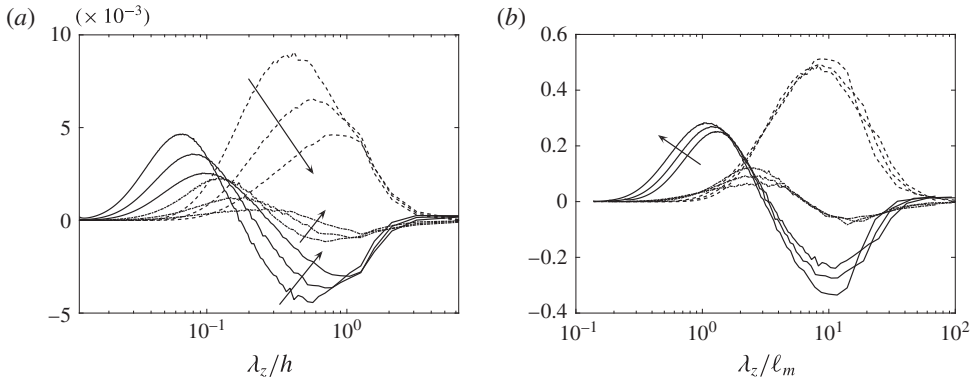
FIGURE 7. Premultiplied one-dimensional cospectra as functions of λ_z in the overlap layer $y^+ > 110$ and $y/h < 0.3$ for C900. The arrows indicate the direction of the increase in y. — —, production rate; ——, spatial transport; — · —, interscale transport.

is scaled by Kolmogorov's length scale, which increases more slowly compared to ℓ_m. The magnitude of the contribution in the overlap layer is scaled well by the total production rate at each height. As shown in figure 7(b), the contribution of the spatial transport is weaker than the contributions of the production, dissipation and interscale transport. Though the downward spatial fluxes have a large impact on the budget in the vicinity of the wall, these three contributions almost complete the budget at each height in the overlap layer, at least in the sense of average for the presented range of Reynolds numbers.

It is observed that the scales of spatial turbulent transport are given by ℓ_m in the overlap layer, which supports the classical assumption of the linearity of y in the logarithmic layer because $\ell_m \to \kappa y$ for high Reynolds numbers. This implies that its structures are self-similar, as are those of momentum transport. Spatial transport is active in the energy-containing range, and its length scale separates more from the dissipation range for higher y in the logarithmic layer. Kolmogorov's law for the energy spectrum would be observed for a much higher Reynolds number where these two scales show sufficient separation.

The structures of momentum transport are invariant against the Reynolds number (Lozano-Durán *et al.* 2011), and this also seems true for spatial turbulent transport. Figure 8 compares the cospectra of spatial turbulent transport and spatial energy fluxes for C500 and C900 in the overlap layer. The cospectra for different Reynolds numbers agree fairly well except at large scales, approximately for $\lambda_z^+ > 10^3$, in the present cases.

5. Pressure–strain correlations

Though the contribution from transport by pressure, $d\overline{pv}/dy$, to the energy budget is weak, except for the near-wall region (Mansour *et al.* 1988; Hoyas & Jiménez 2008), the role of pressure in energy transport is important because it redistributes energy from u to v and w. Energy is first fed into u from the mean shear, and approximately half of that is distributed to the other components. The budget equations for the normal Reynolds stresses $\overline{u_i^2}$ include pressure–strain correlations $\overline{p(\partial u_i/\partial x_i)}$, which represent the rate of energy exchange between the components. The terms $\overline{p(\partial v/\partial y)}$ and $\overline{p(\partial w/\partial z)}$ are actual energy sources for the wall-normal and spanwise components.
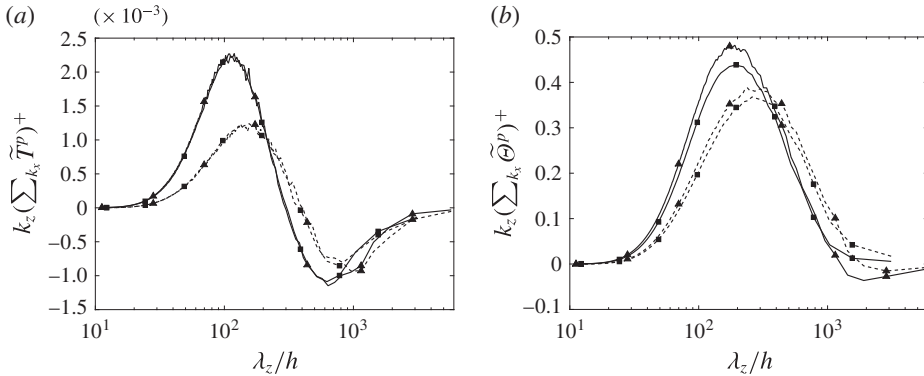
FIGURE 8. Premultiplied one-dimensional cospectra of (*a*) spatial turbulent transport and (*b*) spatial flux as functions of λ_z at $y^+ = 110$ (——) and 150 (— —) for C500 and C900. The symbols indicate the Reynolds number as shown in table 1. The magnitudes are normalised by the wall unit.

The root mean square of the pressure fluctuations on the wall is not scaled by the wall unit (Hu, Morfey & Sandham 2006). This may be explained by the fact that the Green functions of the Poisson equation for low wall-parallel wavenumbers have a long tail in the wall-normal direction. The effect of the source away from the wall is global, and reaches the vicinity of the wall (Kim 1989). The spectrum of the time sequence is not scaled well by a single representative time scale, but is scaled well by the inner (outer) scale for high (low) frequency modes (Hu *et al.* 2006). It is also found that the mean-squared pressure fluctuation exhibits logarithmic dependence on the wall distance (Jiménez & Hoyas 2008). These observations may imply that pressure fluctuations consist of *Re*-dependent and -independent motions as well as *u* and *w* components of velocity fluctuations. In contrast, the spectra of pressure fluctuations in the logarithmic layer are rather isotropic, and the peak of the intensity near the wall is scaled well in the unit given by the local Reynolds shear stress, which suggests that the structures of pressure fluctuations are rather local in the wall-normal direction (Jiménez & Hoyas 2008).

It is also known that pressure–strain correlations are not scaled well near the wall (Hoyas & Jiménez 2008). As shown in figure 9(*a*), these correlations in the wall unit increase with the Reynolds number. The failure of wall scaling is significant in the viscous sublayer, where the energy is transferred from *v* to *w*. The cospectrum of pressure–strain correlations

$$\widetilde{\Pi}_j^s(\boldsymbol{k}, y) = \mathrm{Re}\{\langle (\partial_j \widehat{u}_j)\widehat{p}^* \rangle\}, \tag{5.1}$$

for $j = 1, 2$ and 3 give us the scale dependence of the rate of energy exchange between the velocity components. These three cospectra balance; that is,

$$\sum_{i=1}^{3} \widetilde{\Pi}_i^s(\boldsymbol{k}, y) = 0, \tag{5.2}$$

for all $\boldsymbol{k}$ and y because of the continuity, $\sum_j \partial_j \widehat{u}_j = 0$. Figure 9(*b*) shows the premultiplied two-dimensional cospectrum $\widetilde{\Pi}_2^s$ at $y^+ = 2$. No clear indication of
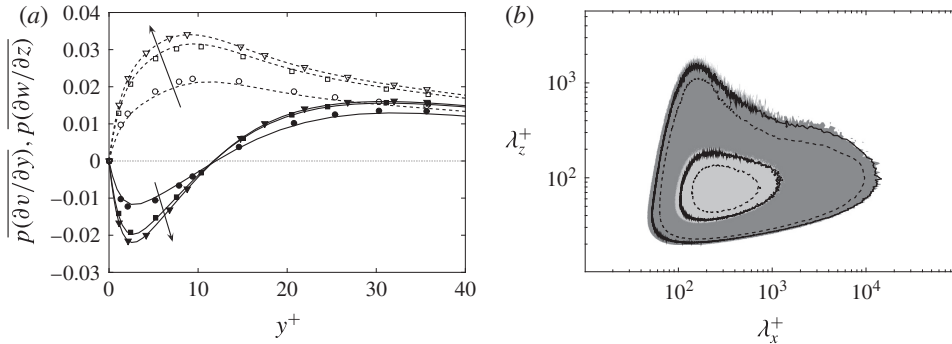
FIGURE 9. (*a*) Total pressure–strain correlations near the wall in the wall unit. The symbols indicate the Reynolds number as shown in table 1. Filled and open symbols are respectively $\overline{p(\partial v/\partial y)}$ and $\overline{p(\partial w/\partial z)}$. Lines are the numerical data for $Re_\tau = 180$, 550 and 950 (Hoyas & Jiménez 2008). The arrows indicate the increase in Reynolds number. (*b*) Premultiplied two-dimensional cospectra of pressure–strain $\widetilde{\Pi}_2^s$ at $y^+ = 2$. Shaded, C900; ———, C500; — —, C200.

the invasion of large-scale structures into the viscous sublayer is observed in the cospectrum, at least for the present range of Reynolds numbers. The cospectra do not have a tail extending toward larger scales as the Reynolds number increases, but the magnitude just increases at all the scales.

Above $y^+ \approx 50$, the structure of the cospectra of pressure–strain correlations does not change qualitatively and is almost isotropic. In the buffer layer, their characteristic length scale is approximately $\lambda_x^+ \approx \lambda_z^+ \approx 200$, which is independent of the Reynolds number. The relevant length scale of the correlations increases with the wall distance in the overlap layer, as seen in figure 10(*a*). The cospectra at different heights perfectly collapse when the wavelength is normalised by ℓ_m and the magnitude is normalised by the production rate at each height, as shown in figure 10(*b*). Because the length scale is represented well by ℓ_m, the structures involved in the energy exchange between the velocity components are localised in the wall-normal direction, and are not affected by large-scale structures.

The cospectra of the pressure–strain correlations are characterised by the aspect ratio in the wall-parallel dimensions. We here define the one-dimensional cospectra as a function of the modified aspect ratio $a \equiv \log \lambda_z / \log \lambda_x$,

$$\widetilde{\Pi}_i^s(a, y) = \sum_{\lambda_x^a = \lambda_z} \widetilde{\Pi}_i^s(\boldsymbol{k}, y). \tag{5.3}$$

The structure of the redistribution near the wall is distinguished because the energy is transferred from v to w, as seen in the one-point budget in figure 9(*a*). The balance as a function of a is given by figure 11(*a*). Energy transfer from v to w is involved in the flow structures elongated in x, satisfying $\lambda_z = \lambda_x^{0.7}$ or $\lambda_x^{0.8}$. The cospectra drastically evolve within a short range in y. At $y^+ = 15$, energy is provided from u mainly to w for $a \approx 0.9$ that is almost isotropic. The wall-normal component v receives a little energy from w through elongated structures, approximately $\lambda_z = \lambda_x^{0.6}$ or $\lambda_x^{0.7}$. The two cases for higher Reynolds numbers agree well. As mentioned earlier, the cospectra in the buffer layer are universal. Above the overlap layer, the energy is redistributed from u to the other components around $a = 1$. As in the case of $y^+ = 15$, v receives
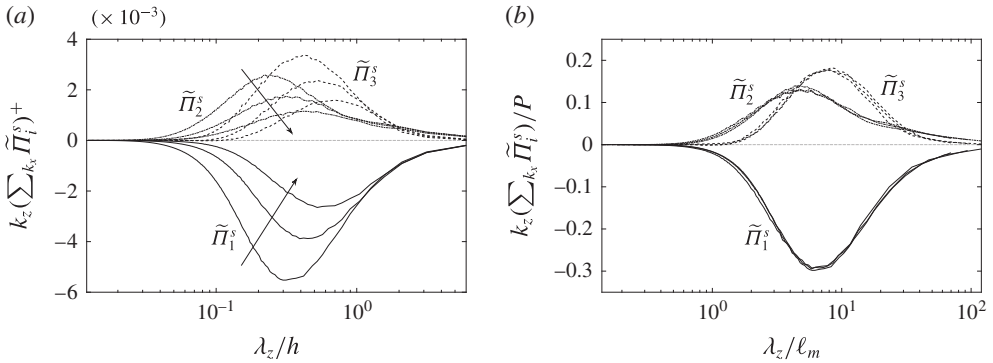
FIGURE 10. Premultiplied one-dimensional cospectra of pressure–strain correlations as functions of (*a*) λ_z/h and (*b*) λ_z/ℓ_m at $y^+ = 110$, 150 and 220 for C900. ——, $k_z \sum_{k_x} \widetilde{\Pi}_1^s$; — · —, $k_z \sum_{k_x} \widetilde{\Pi}_2^s$; ——, $k_z \sum_{k_x} \widetilde{\Pi}_3^s$. The magnitude is normalised by (*a*) the wall unit and (*b*) the total production rate at each height. The arrows in (*a*) indicate the increase in Reynolds number.

energy from w as well through elongated structures. The total energy provided to v and w is approximately the same, but the aspect ratio of the fluctuations gained for v is wider than that for w. In addition, at this height, the two higher cases collapse fairly well. In the outer layer, the structure of redistribution is qualitatively same, but the magnitude is scaled by the outer unit u_τ^3/h.

6. Conclusions

The constituents of the spectral energy budget equation have been evaluated by DNS data to examine their scale dependence. In the buffer layer, downward fluxes emerge at large scales. These fluxes originate in the overlap layer and carry energy to the vicinity of the wall. The range of the scales at which these downward fluxes are intense become wider for larger Reynolds numbers. The accumulated energy carried by the fluxes leads to *Re* dependence of the intensity of wall-parallel velocity fluctuations and the dissipation rate near the wall.

The upward energy fluxes above the buffer layer provide energy to narrower scales but remove it from wider scales. In the overlap layer, the cospectrum of the spatial turbulent transport is scaled well by the mixing length. This shows that the structures of fluctuations involved in turbulent transport are self-similar. In addition, they do not depend on the Reynolds number.

To understand the overall structure of the energy budget requires considering spatial transport (Tuerke & Jiménez 2013). Spatial transport plays an important role, as has been discussed, but the intensity of its contribution to the budget at each height is weak compared to production and dissipation in the overlap region. Because interscale turbulent transport carries only large to small scales on average, a net supply of energy to the scales larger than the scales of production is not available. On the other hand, the individual dynamics of structures may imply the evolution from small to large scales (Lozano-Durán & Jiménez 2014*b*). In accordance with this dynamics, energy transport from small to large scales occurs, but it is always cancelled by another event that causes large-scale structures to break down to smaller-scale ones. Unfortunately, such individual events sustaining the energy spectra are hidden in the present analysis, where only the net energy transfer is visible.
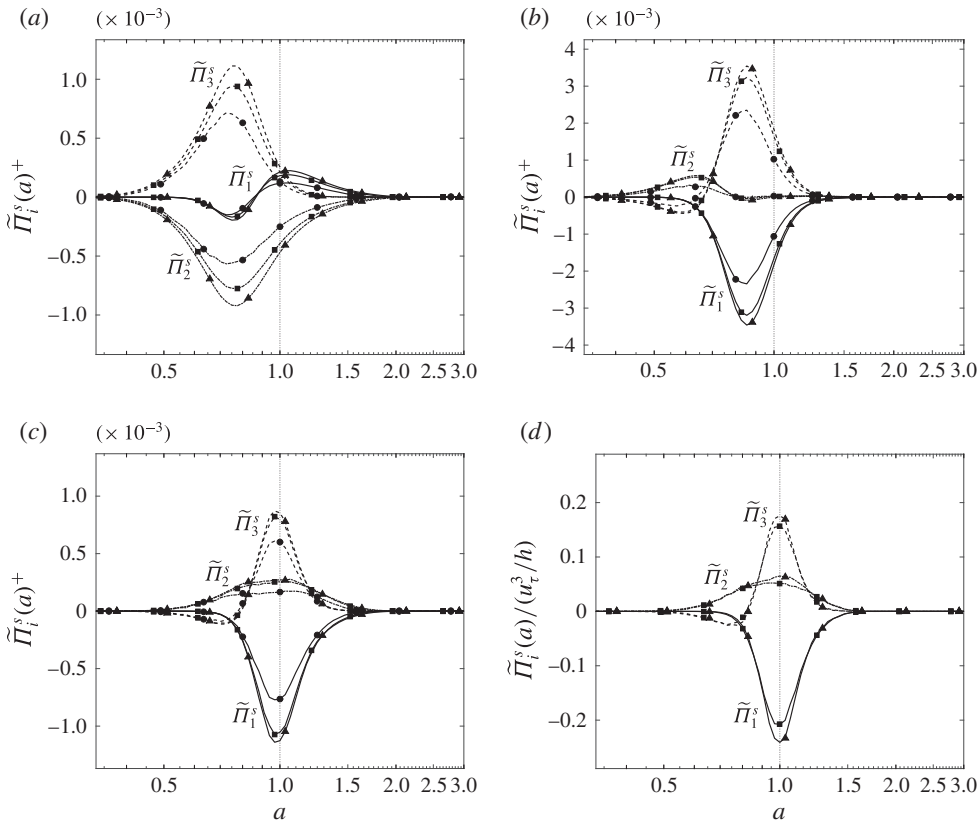
FIGURE 11. Cospectra of pressure–strain correlations as functions of the aspect ratio $a = \log \lambda_z^+ / \log \lambda_x^+$ at (a) $y^+ = 1$, (b) 15, (c) 110 and (d) $y/h = 0.5$. ——, $\widetilde{\Pi}_1^s$; — · —, $\widetilde{\Pi}_2^s$; ——, $\widetilde{\Pi}_3^s$. The symbols indicate the Reynolds number as shown in table 1.

The cospectra of the pressure–strain correlations are also evaluated. They are not scaled by the wall unit near the wall, but no indication of the influence of large scales is observed in the cospectra, at least for the present range of Reynolds numbers. Above the buffer layer the cospectra of the pressure–strain correlations are almost isotropic, and their relevant length scale is given by the mixing length in the overlap layer. The pressure–strain correlations are therefore rather local quantities.

Acknowledgements

REFERENCES

DEL ÁLAMO, J. C., JIMÉNEZ, J., ZANDONADE, P. & MOSER, R. D. 2004 Scaling of the energy spectra of turbulent channels. *J. Fluid Mech.* **500**, 135–144.

BOLOTNOV, I. A., LAHEY, R. T. JR, DREW, D. A., JANSEN, K. E. & OBERAI, A. A. 2010 Spectral analysis of turbulence based on the DNS of a channel flow. *Computers Fluids* **39**, 640–655.

BRADSHAW, P. 1967 'Inactive' motion and pressure fluctuations in turbulent boundary layers. *J. Fluid Mech.* **30**, 241–258.

CIMARELLI, A., ANGELIS, E. DE & CASCIOLA, C. M. 2013 Paths of energy in turbulent channel flows. *J. Fluid Mech.* **715**, 436–451.

CIMARELLI, A., ANGELIS, E. DE, JIMÉNEZ, J. & CASCIOLA, C. M. 2016 Cascades and wall-normal fluxes in turbulent channel flows. *J. Fluid Mech.* **796**, 417–436.

CIMARELLI, A., ANGELIS, E. DE, SCHLATTER, P., BRETHOUWER, G., TALAMELLI, A. & CASCIOLA, C. M. 2015 Sources and fluxes of scale energy in the overlap layer of wall turbulence. *J. Fluid Mech.* **771**, 407–423.

DEGRAAFF, D. B. & EATON, J. K. 2000 Reynolds-number scaling of the flat-plate turbulent boundary layer. *J. Fluid Mech.* **422**, 319–346.

DOMARADZKI, J. A., LIU, W., HÄRTEL, C. & KLEISER, L. 1994 Energy transfer in numerically simulated wall-bounded turbulent flows. *Phys. Fluids* **6**, 1583–1599.

DUNN, D. C. & MORRISON, J. F. 2003 Anisotropy and energy flux in wall turbulence. *J. Fluid Mech.* **491**, 353–378.

DUNN, D. C. & MORRISON, J. F. 2005 Analysis of the energy budget in turbulent channel flow using orthogonal wavelets. *Computers Fluids* **34**, 199–224.

FLORES, O. & JIMÉNEZ, J. 2006 Effect of wall-boundary disturbances on turbulent channel flows. *J. Fluid Mech.* **566**, 357–376.

FLORES, O. & JIMÉNEZ, J. 2010 Hierarchy of minimal flow units in the logarithmic layer. *Phys. Fluids* **22**, 071704.

HAMILTON, J. M., KIM, J. & WALEFFE, F. 1995 Regeneration mechanisms of near-wall turbulence structures. *J. Fluid Mech.* **284**, 317–348.

HOYAS, S. & JIMÉNEZ, J. 2008 Reynolds number effects on the Reynolds-stress budgets in turbulent channels. *Phys. Fluids* **20**, 101511.

HU, Z. W., MORFEY, C. L. & SANDHAM, N. D. 2006 Wall pressure and shear stress spectra from direct simulations from channel flow. *AIAA J.* **44**, 1541–1549.

HUTCHINS, N. & MARUSIC, I. 2007 Evidence of very long meandering features in the logarithmic region of turbulent boundary layers. *J. Fluid Mech.* **579**, 1–28.

JIMÉNEZ, J. 1999 The physics of wall turbulence. *Physica A* **263**, 252–262.

JIMÉNEZ, J. 2012 Cascades in wall-bounded turbulence. *Annu. Rev. Fluid Mech.* **44**, 27–45.

JIMÉNEZ, J. & HOYAS, S. 2008 Turbulent fluctuations above the buffer layer of wall-bounded flows. *J. Fluid Mech.* **611**, 215–236.

JIMÉNEZ, J. & PINELLI, A. 1999 The autonomous cycle of near-wall turbulence. *J. Fluid Mech.* **389**, 335–359.

KIM, J. 1989 On the structure of pressure fluctuations in simulated turbulent channel flow. *J. Fluid Mech.* **205**, 421–451.

KIM, J., MOIN, P. & MOSER, R. D. 1987 Turbulence statistics in fully developed channel flow at low Reynolds number. *J. Fluid Mech.* **177**, 133–166.

LEE, M. 2015 Direct numerical simulation (DNS) for incompressible turbulent channel flow at $Re_\tau = 5200$. PhD dissertation, The University of Texas at Austin, Austin, Texas.

LEE, M. & MOSER, R. D. 2015*a* Direct numerical simulation of turbulent channel flow up to $Re_\tau \approx 5200$. *J. Fluid Mech.* **774**, 395–415.

LEE, M. & MOSER, R. D. 2015*b* Spectral analysis on Reynolds stress transport equation in high *Re* wall-bounded turbulence. In *International Symposium on Turbulence and Shear Flow Phenomena (TSFP-9)*, pp. 4A–3. Melbourne.

LOZANO-DURÁN, A., FLORES, O. & JIMÉNEZ, J. 2011 The three-dimensional structure of momentum transfer in turbulent channels. *J. Fluid Mech.* **694**, 100–130.

LOZANO-DURÁN, A. & JIMÉNEZ, J. 2014*a* Effect of the computational domain on direct simulations of turbulent channels up to $Re_\tau = 4200$. *Phys. Fluids* **26**, 011702.

LOZANO-DURÁN, A. & JIMÉNEZ, J. 2014*b* Time-resolved evolution of coherent structures in turbulent channels: characterization of eddies and cascades. *J. Fluid Mech.* **759**, 432–471.

LUMLEY, J. L. 1964 Spectral energy budget in wall turbulence. *Phys. Fluids* **7**, 190–196.

MANSOUR, N. N., KIM, J. & MOIN, P. 1988 Reynolds-stress and dissipation-rate budgets in a turbulent channel flow. *J. Fluid Mech.* **194**, 15–44.

MARATI, N., CASCIOLA, C. M. & PIVA, R. 2004 Energy cascade and spatial fluxes in wall turbulence. *J. Fluid Mech.* **521**, 191–215.

MATHIS, R., HUTCHINS, N. & MARUSIC, I. 2009 Large-scale amplitude modulation of the small-scale structures in turbulent boundary layers. *J. Fluid Mech.* **628**, 311–337.

METZGER, M. M. & KLEWICKI, J. C. 2001 A comparative study of near-wall turbulence in high and low Reynolds number boundary layers. *Phys. Fluids* **13**, 692–701.

MIZUNO, Y. & JIMÉNEZ, J. 2011 Mean velocity and length-scales in the overlap region of wall-bounded turbulent flows. *Phys. Fluids* **23**, 085112.

MIZUNO, Y. & JIMÉNEZ, J. 2013 Wall turbulence without walls. *J. Fluid Mech.* **723**, 429–455.

MONTY, J. P., STEWART, J. A., WILLIAMS, R. C. & CHONG, M. S. 2007 Large-scale features in turbulent pipe and channel flows. *J. Fluid Mech.* **589**, 147–156.

TENNEKES, H. & LUMLEY, J. L. 1972 *A First Course in Turbulence*. MIT Press.

TUERKE, F. & JIMÉNEZ, J. 2013 Simulations of turbulent channels with prescribed velocity profiles. *J. Fluid Mech.* **723**, 587–603.